JAAS

ROYAL SOCIETY OF CHEMISTRY

PAPER

View Article Online
View Journal | View Issue

Cite this: J. Anal. At. Spectrom., 2025, 40, 1220

Investigating the mechanism that reduces the memory effect of Li on MC-ICP-MS†

Tiantian Zhang,[a] Jie Lin, *[a] Xi Zhu,[a] Ao Yang,[a] Kexin Deng,[a] Zhaochu Hu[ab] and Yongsheng Liu[c]

The memory effect significantly impacts the precision and accuracy of lithium isotope measurements using MC-ICP-MS. This study evaluates the origin of the memory effect, identifying the cones, especially the skimmer cone, as the primary site responsible for lithium memory accumulation. To investigate the type and optimal concentration of sodium-containing solutions, scanning electron microscope (SEM) and cone elution experiments were conducted. Results demonstrated that a 0.5% $NaNO_3$ solution was the most effective based on the high signal-to-blank ratio, less impacted signal intensity and non-interferences. Combined with the SEM results and KCl elution experiments, the mechanism by which the Na solution reduces the lithium memory effect can be attributed to two aspects. First, a nanoscale particle coating is formed on the cone surface, preventing the deposition of Li material on the cone. Second, Na/K solutions are preferentially ionized due to their low ionization energies, reducing or even eliminating the ionization of the analyzed Li. Based on these findings, we infer that high-concentration rinse solutions of alkali or alkaline earth metals may effectively reduce the memory effect of other related elements.

Received 23rd January 2025
Accepted 17th March 2025

DOI: 10.1039/d5ja00031a

rsc.li/jaas

1. Introduction

Lithium (Li) has two stable isotopes (^{6}Li and ^{7}Li), with natural abundances of 7.52% and 92.48%, respectively. Their significant mass difference of 16.7% results in notable isotopic fractionation during various geological processes, including weathering, magmatic differentiation, hydrothermal alteration, and crust-mantle cycling.[1–18] As a result, Li isotopes are widely used as tracers in studies of continental weathering, rock origins, and the mechanisms of deposit formation.

For geological applications, accurate and precise measurement of Li isotopic compositions is essential. Multi-collector inductively coupled plasma mass spectrometry (MC-ICP-MS) has become the preferred method for Li isotope determination owing to its high ionization efficiency, effective sample introduction, minimal matrix effects, and excellent instrument stability.[19–24] However, the accuracy of Li isotope analysis on MC-ICP-MS is often compromised by significant instrumental background and memory effects. Li blanks are difficult to remove and tend to accumulate during measurement (20–200 mV).[25] Additionally, the Li isotopic composition of the blank (δ^7Li: −200‰ to −450‰)[25,26] differs substantially from that of geological samples (δ^7Li: −10‰ to −50‰),[27,28] leading to considerable errors if blank corrections are not properly corrected due to the memory effect. For example, Tomascak *et al.*[29] found that without blank correction during Li isotope measurements, the actual sample value decreases by 0.24‰.

The most commonly used method to reduce the Li memory effect is to extend the washing time,[30,31] typically using cleaning solutions such as Milli-Q water or 2% HNO_3. However, increasing the wash time from 15–20 s to 240 s results in reduced experimental efficiency and extends the time gap between sample and standard measurements, which compromises the accuracy of sample-standard bracketing.[32,33] Alternatively, changing the cleaning solution can also reduce Li memory effects. Liu *et al.*[34] proposed a sequence of 1% HF + 2% HNO_3, 1% HNO_3 + 5% HCl, and 2% HNO_3 to eliminate Li memory effects, while Gou *et al.*[35] recommended using 5% HNO_3, 0.1% HF, and 2% HNO_3, despite HF causing wear to the spray chamber and torch. Lin *et al.*[36] introduced a more effective method involving flushing the system with a 5% NaCl solution for 1 min, which significantly reduces the Li memory effect by lowering the background Li signal by two orders of magnitude, while maintaining stable signal intensities for up to 3 h. This method improves the cleaning efficiency of the instrument background by three to five times. It has been widely adopted by numerous institutions, including the University of Cambridge, Indian Institute of Science, and Thermo Fisher Scientific,

[a]State Key Laboratory of Geological Processes and Mineral Resources, School of Earth Sciences, China University of Geosciences, Wuhan 430074, China. E-mail: linjie@cug.edu.cn; Fax: +86-27-67885096; Tel: +86-27-87483044

[b]Faculty of Materials Science and Chemistry, China University of Geosciences, Wuhan 430074, P. R. China

[c]Yangtze University, Jingzhou 434000, P. R. China

† Electronic supplementary information (ESI) available. See DOI: https://doi.org/10.1039/d5ja00031a

Guiyang Institute of Geochemistry, Chinese Academy of Sciences.[37–52] Bohlin *et al.*[39] refined this method, suggesting that 10 μg per g of NaCl can still significantly reduce the Li memory effect in the Neptune Plus MC-ICP-MS system. Their study demonstrated that pre-conditioning the system with NaCl solution for 10 min reduced the blank from 100 mV to 0.5–3 mV. This approach was effectively applied in the Nu Plasma MC-ICP-MS for Li isotope determination. Tang *et al.*[53] further recommended using 0.3% NaCl for 60 s, which significantly reduced the background Li signal in Nu Plasma instrument.

Further research shows that Be, B, Na, Cl, K, Zr, Pt, and U elements are affected by the memory effect.[24,54–60] Consequently, the memory effect is recognized as a widespread phenomenon that impacts the accurate simultaneous determination of multiple elements, not only Li. The discovery that NaCl can reduce the memory effect of Li is expected to provide significant insights into the reduction of memory effects for other elements. Therefore, it is crucial to elucidate the mechanism by which NaCl reduces the memory effect. The study of the mechanism will also influence the selection of the optimal concentration. Lin *et al.*[36] hypothesized that a thin "Na coating film" forms in the interface system after introducing concentrated NaCl solution, which prevents or reduces Li deposition on the cones. In addition to NaCl, other solutions used for cone coating include urine,[61] Si solutions,[62] and Be solutions.[63] Rodushkin *et al.*[61] pointed out that injecting ten-fold diluted urine for 10–15 min before sample analysis forms a salt crust on the cone, which can reduce the deposition of elements on the cone. Engström *et al.*[62] utilized a 0.2% Si solution to coat the cone for 10 min to determine the elemental content in biological soft tissues. This method reduces background signals, and the oxide yield fell from 2.5% to 1%. Therefore, researching the mechanism to reduce the memory effect of Li and other elements is of great significance.

This study investigated the mechanism by which NaCl reduces the Li memory effect. Scanning electron microscopy (SEM) analysis of the cone surface and the observation of the distribution of ions reveals a thin deposited film. Cone elution experiments were performed to wash off the ions from the cone surface, followed by elemental analysis of major and trace elements to differentiate between the inner and outer deposits. A gradient experiment was designed to explore the effect of 0.05%, 0.5%, 1%, and 5% NaCl concentrations. A comparative experiment using $NaNO_3$ and NaCl was conducted to determine whether Na^+ or Cl^- is primarily responsible for the observed effects. Additionally, the underlying mechanism was further investigated by comparing the ionization energies of KCl and NaCl.

2. Experimental section

2.1 Instrumentation

Lithium isotope analysis was conducted using a double-focusing MC-ICP-MS instrument (Neptune Plus, Thermo Fisher Scientific, Germany) at the State Key Laboratory of

Table 1 Instrumental parameters for MC-ICP-MS and ICP-MS/MS

MC-ICP-MS	Li isotopic analysis
Parameter	Value
Resolution	Low (∼400)
Power (W)	1200
Cooling gas (L min^{-1})	16.0
Auxiliary gas (L min^{-1})	1.21
Sample gas (L min^{-1})	0.984
Integration time (s)	4.194
Cone type	Jet + X
Zoom optics (V)	Focus quad: −4; dispersion quad: 17.6
Focusing lens voltage (V)	Focusing lens: −5; dispersing lens: 17.6
Sensitivity (V μg per g (^{7}Li))	100–130
Background signal (2% HNO_3) (mV)	Without NaCl: 53–180; with NaCl: 6–16
Agilent 8900	**Elemental analysis**
RF power (W)	1550
Sampling depth (mm)	8
Plasma gas flow rate (L min^{-1})	15
Carrier gas flow rate (L min^{-1})	1.09
Extraction 1 lens (V)	−2.7
Extraction 2 lens (V)	−250
Omega bias lens (V)	−150
Omega lens (V)	11.6
Q1 bias (V)	−1.0
Octopole bias (V)	−5.0
Q2 bias (V)	−12.0
Integration time (s per isotope)	0.3
Replicates	3

Geological Processes and Mineral Resources (GPMR), China University of Geosciences (Wuhan). The instrument is equipped with nine movable Faraday cups, with $^{7}Li/^{6}Li$ measured in the H4 and L5 cups, respectively. Detailed instrument parameters are shown in Table 1. Sample solutions were introduced using a stable sample introduction system ($\sim$100 μL min^{-1}) equipped with a PFA nebulizer, a quartz spray chamber, and an autosampler (SX-112FR). Ni "Jet + X" cone combinations with orifice diameters of 1.2 mm and 0.7 mm were used, achieving an instrumental sensitivity of 100–130 V μg^{-1} g^{-1} (^{7}Li).

The SEM experiments were performed using a field emission scanning electron microscope (FEG-SEM). Backscattered electron (BSE) images of the nickel cone deposits were captured with a Zeiss Sigma 300 FEG-SEM, operated at an accelerating voltage of 20 kV, a beam current of 20 nA, a working distance of 8–15 mm, and a beam spot size of approximately 1 μm.

Major and trace element analyses of the cone deposits were conducted using an Agilent 8900 ICP-MS/MS. Detailed instrument parameters are listed in Table 1. Data acquisition was obtained using a single internal standard (In) and multiple external standards for calibration. Before testing, samples were diluted with 2% HNO_3 to a final volume of 2 mL. A laboratory internal quality control sample (QC) was inserted every 10 samples to correct for time drift and monitor long-term quality. Element concentrations were obtained online based on the calibration curve, and further corrected offline using the ICPMSDataCal software.[64]

2.2 Reagents and solutions

The lithium isotope standards used in this study included the internationally recognized L-SVEC standard (pure Li_2CO_3) and the high-purity plasma standard solution Alfa-Li from Alfa Aesar (China). Approximately 50 mg of L-SVEC powder was dissolved in 2 mL of concentrated nitric acid, evaporated to dryness, and then diluted with 2% nitric acid to produce a solution of approximately 20 μg per g. Before analysis, the solution was further diluted with 2% nitric acid to the appropriate concentration. The L-SVEC Li solution (20 μg per g) was diluted with 2% nitric acid to prepare 100 ng per g and 200 ng per g solutions. Similarly, Alfa-Li (1000 μg per g) was diluted with 2% nitric acid to prepare a 200 ng per g solution. BHVO-2 (basalt) used to estimate the effect of accurate blank subtraction was from United States Geological Survey (USGS).

The preparation of reagents and sample digestion were all conducted in a class-100 cleanroom. Nitric acid used was purified through a DST-1000 acid purification system (Savillex) using double sub-boiling distillation. Ultrapure water was obtained using a Milli-Q Element purification system (Millipore Corp. Billerica, MA, USA), with a resistivity of 18.2 MΩ. All beakers and disposable plastic containers such as pipette tips, sample introduction tubes, and centrifuge tubes used during the experiments were acid-washed and rinsed with Milli-Q water. To reduce the memory effect of Li, a 5% NaCl solution was prepared by diluting 5 g of ≥99.99% NaCl powder in ultrapure water to a total of 100 g. The optimal NaCl concentration was determined by testing diluted 5% NaCl solutions (0.05%, 0.5%, and 1%). A 0.5% $NaNO_3$ solution was prepared by evaporating a 1000 μg per g sodium single-element standard to dryness, followed by medium conversion with nitric acid. KCl powder (≥99.99%) was dissolved with ultrapure water to prepare 0.05%, 0.1%, 0.5%, and 5% solutions to evaluate their effectiveness in reducing Li memory effect. The Na single-element standard was purchased from China Iron & Steel Research Institute Group (CISRI).

3. Results and discussion

3.1 Impact of the Li memory effect on the isotopic accuracy

To investigate the existence and impact of the lithium (Li) memory effect, experiments were conducted using two solutions with significantly different Li isotopic compositions: L-SVEC (0.00‰ ± 0.25‰),[36] and Alfa-Li (105.33‰ ± 0.39‰).[65] The measurement sequence was as follows: Blk—L-SVEC—Blk—Alfa-Li—Blk—L-SVEC—Blk—Alfa-Li—Blk to assess the blank (Blk) Li isotopic composition and the background signal intensity. The Li signal intensity in the blank solution increased over time. Furthermore, the Li isotopic composition of each blank measurement was influenced by the composition of the preceding solution. Specifically, the blank Li isotopic composition was consistently higher after measurements with the Alfa-Li solution compared to those following L-SVEC. This pattern provides strong evidence for the presence of a significant Li memory effect, as both the increasing Li blank signal and the influence of the preceding solution's composition were clearly observed (Fig. 1).

To minimize the impact of the memory effect on Li isotopic measurements, a blank subtraction is commonly employed. However, the existence of a memory effect makes it difficult to obtain true blank values, as there can be significant discrepancies between the actual blank Li isotopic composition and that of the sample. This difficulty can introduce substantial errors when accurate blank subtraction is not possible. For example, Tomascak *et al.*[66] reported a Li process blank of 610 pg with an isotopic composition of $\delta^{7}Li \sim +20‰$. For a sample containing 40 ng of Li, the isotopic bias could reach 0.24‰ if blank subtraction was not performed accurately. Elburg *et al.*[67] consolidated methods for blank subtraction in solution-based measurements and highlighted that failure to perform precise blank correction could significantly impact the precision and accuracy of isotopic composition determinations.

Eqn (1) can be used to estimate the effect of accurate blank subtraction on Li isotopic measurements. The sample analyzed is assumed to be BHVO-2 ($\delta^{7}Li = 4.50‰ \pm 0.24‰$,[36] while the isotopic composition of the blank is represented by the long-term monitoring value from laboratory data, which is $-329.75‰ \pm 258.08‰$ (2SD, $n = 535$). The Li content for BHVO-2 varied at 0.5, 1, 5, 10 and 100 ng, with blank Li mass ranging from 0 to 0.05 ng. Using eqn (1), errors resulting from inaccurate blank subtraction become more pronounced as the sample amount decreases (Fig. 1b). For example, the isotopic bias introduced by inaccurate blank subtraction could reach 2.38‰ if the sample contains 10 ng of Li and the blank Li mass is 0.05 ng. This bias would exceed the laboratory's long-term

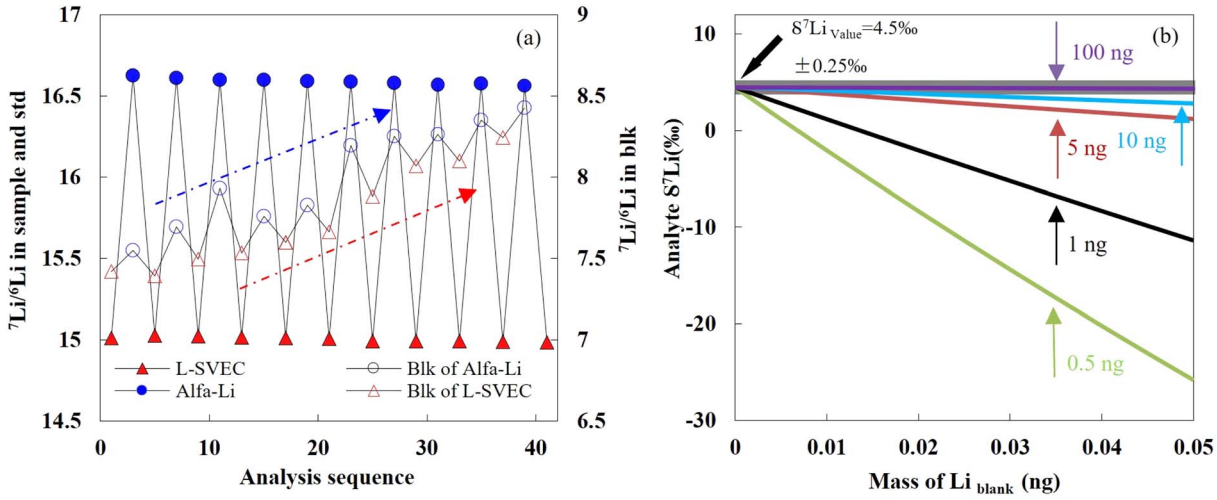

Fig. 1 (a) Monitoring Li isotopic composition ($^7Li/^6Li$) for L-SVEC and Alfa-Li blanks. (b) Simulation of experimental error introduced by blank contributions during lithium measurements. The *x*-axis represents the mass of lithium in the blank, while the *y*-axis displays the combined lithium isotopic composition resulting from the blank and the sample. The green, black, red, blue, and purple lines represent 0.5, 1, 5, 10, and 100 ng sample masses, respectively.

measurement precision of 0.24‰,[36] severely impacting measurement accuracy.

To achieve a true blank value, one effective method is to extend the wash time to mitigate the memory effect. However, this approach reduces experimental efficiency and increases the time interval between sample and standard measurements, which negatively affects the accuracy of correction through sample-standard bracketing.[68] Alternative methods such as linear interpolation accurately assess blanks in the presence of significant memory effects.[69,70] For example, Kimura *et al.*[70] measured 30 blank Li values before and 15 values after sample measurements, applying linear interpolation to the blanks for the 34 samples analyzed in between. This time-dependent blank correction method mitigated the influence of the Li memory effect. Nevertheless, the most reliable strategy to avoid interference from the memory effect in Li isotopic measurements is to investigate the source of the memory effect and eliminate it.

$$R_{sam} = \frac{m_{blk} \times r_{blk} + m_{sam} \times r_{sam}}{m_{blk} + m_{sam}} \quad (1)$$

where R_{sam}, r_{sam} and r_{blk} represent the Li isotopic composition of the sample after blank subtraction, the instrument-measured Li isotopic composition, and the blank Li isotopic composition, respectively. m_{sam} and m_{blk} denote the mass of Li in the sample and the blank, respectively. When applying this equation, it is essential to consider the challenges associated with accurately determining the blank Li mass. This limitation highlights the importance of minimizing the blank signal to the greatest extent possible and ensuring precise blank correction to avoid introducing significant errors into the final isotopic composition.

3.2 Li memory effect on the sampling and skimmer cone

The sample cone and skimmer cone serve as the critical interface between the plasma and the mass spectrometer, facilitating the efficient transmission of ions. At this interface, the plasma expands in a horn-like shape along the outer surface of the sample cone, with most of the ion flux drawn into the cone orifice. The skimmer cone then selects the ion flux exiting the sample cone orifice, allowing it to pass through the skimmer cone orifice into the next stage of the vacuum system. As the ion flux passes through this interface, analyte elements tend to deposit on the surfaces of the sample and skimmer cones. These deposits can re-evaporate and ionize, leading to the memory effect.[25,71–74] For example, Boomer *et al.*[75] reported elemental deposition on the cone surfaces in the measurement of U concentration using solution nebulization (SN)-ICP-MS, where the SEM clearly detected deposits. Similarly, Andrén *et al.*[76] observed that 1% and 6% of the analyzed element were deposited on the sample cone and skimmer cone, respectively during SN-ICP-MS analysis of B. Yang *et al.*[77] also identified elemental deposition on the sample cone and skimmer cone during Sr isotope analysis. Our experiments showed that severe Li memory effects could be mitigated by only replacing the cones, without altering other instrument components such as the spray chamber. After cone replacement, the background Li signal returned to its initial level, confirming that the cones are the primary site of Li memory effect.

To further investigate the specific locations and deposition patterns of Li on the inner and outer surfaces of the cones, three new sets of sample cones (Jet cone) and skimmer cones (X cone) were used. The cones were treated according to the methods outlined in Table 2, and the deposits on the outer surfaces of the sample and skimmer cones were examined for morphological changes after exposure to various solutions using SEM (Fig. 2). Due to the conical shape of the cone tips, SEM light cannot fully penetrate the inner surfaces, limiting effective observation. Therefore, the cones were repeatedly rinsed with 10% HNO_3 to analyze the elemental composition of deposits on the inner and outer surfaces of the cones, and the elemental

Table 2 Injected solutions and deposition of Li for the three different cones

Cone no.	Injected solution	Jet-outside (ng)	Jet-inside (ng)	X-outside (ng)	X-inside (ng)
1	Nothing	—	—	—	—
2	200 ng per g L-SVEC (1 h)	5.3	8.6	178.4	38.8
3	200 ng per g L-SVEC (1 h) → 2% HNO_3 (5 min)	1.9	13	177.2	23.8

concentrations in the rinse solution were measured. The first set of cones was left untreated for comparison (Fig. 2a). The second set of cones was exposed to a continuous inlet of 200 ng per g L SVEC for 1 h to observe Li deposition on the cones to allow a better understanding of the Li memory effect (Fig. 2b). The third set of cones was initially exposed to a continuous inlet of 200 ng per g L SVEC for 1 h, followed by a 5-minute rinse with 2% HNO_3, simulating the conventional cleaning method used

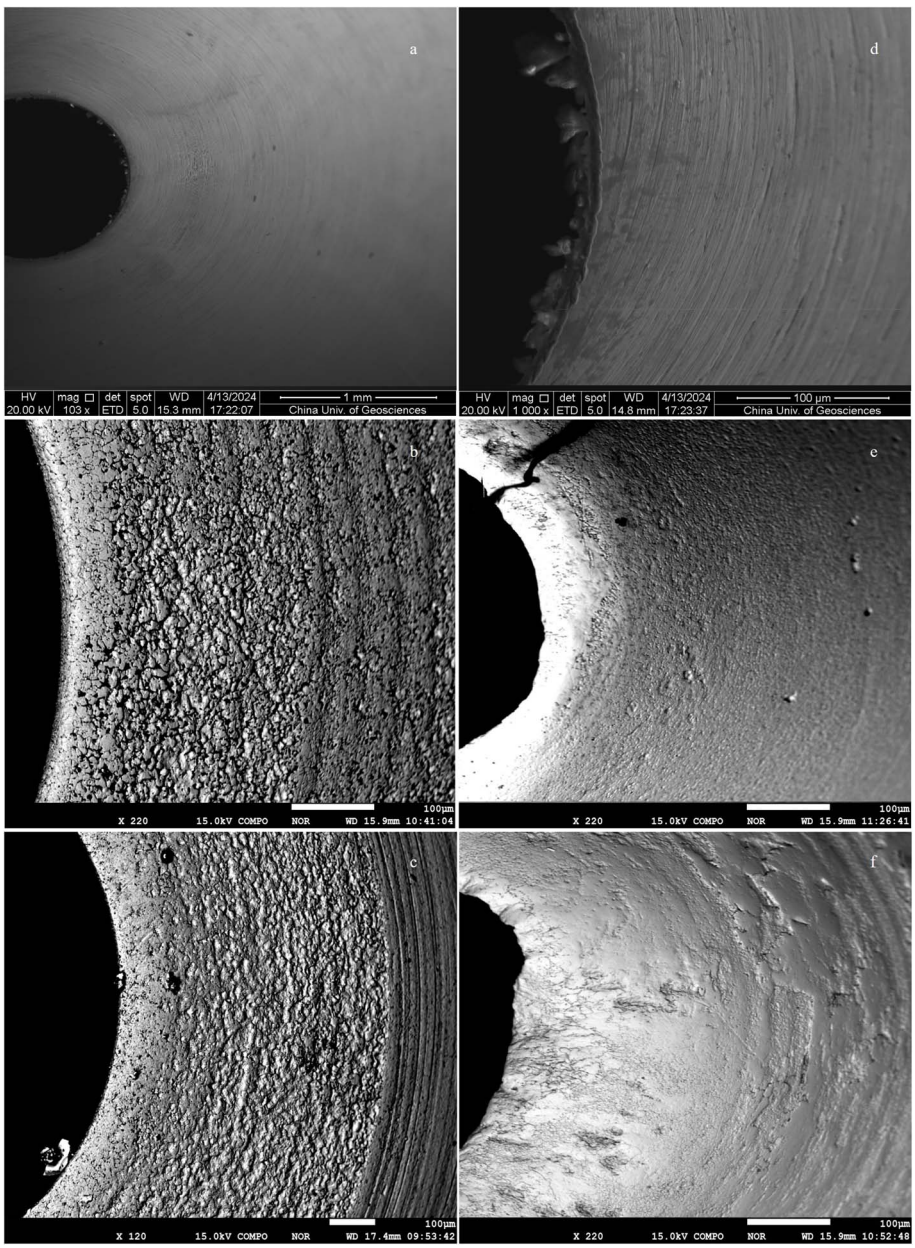

Fig. 2 Exterior of the sampling (left) and skimmer (right) cones following the introduction of various solutions; (a and d) new cones; (b and e) cones treated with 200 ng per g L-SVEC for 1 h; and (c and f) cones treated with 200 ng per g L-SVEC for 1 h, followed by 5 minutes with 2% HNO_3.

in Li isotope analysis. The deposition patterns on the cone surfaces were then analyzed to evaluate the cleaning effectiveness of 2% HNO_3 (Fig. 2c).

SEM observations revealed material deposition on the sample and skimmer cone (Fig. 2). The deposition area and thickness on the outer surface of the skimmer cone were greater than that on the sample cone. Furthermore, cone elution experiments showed that the amount of Li deposited on the inner surface of the skimmer cone (38.8 ng) was significantly higher than that on the inner surface of the sample cone (8.6 ng). Similarly, the Li deposition on the outer surface of the skimmer cone (178.4 ng) exceeded that on the outer surface of the sample cone (8.9 ng). This disparity can be attributed to the thermal and flow dynamics in ICP-MS. The initial temperature of the argon ion source in ICP-MS is approximately 8000–10000 K, and it gradually decreases along the axial direction, reaching about 1700 K near the front wall of the sample cone. Subsequently, particles extracted through the sample cone orifice undergo supersonic expansion. While a small portion of particles pass through to the skimmer cone, the majority collide with the skimmer cone surface, resulting in a larger deposition on the skimmer cone. Lim *et al.*[78] noted that the gas-dynamic temperature in the Mach disk region of the extracted plasma is approximately 2200 K. As the particles approach the skimmer cone, the temperature rapidly decreases to 673–731 K at the skimmer cone tip.[79] During this rapid cooling, condensation of materials from the high-temperature plasma leads to solid deposition on the sample cone and skimmer cone.[71,80] However, condensation is less pronounced on the sample cone due to the relatively higher temperature. Supersonic expansion further disperses particles after passing the sample cone, contributing to a larger deposition area on the skimmer cone.

Significant particle deposition remained visible on the sample cone (Fig. 2c) and skimmer cone (Fig. 2f) even after cleaning with 2% HNO_3 for 5 min. The elution experiments further revealed that 215.9 ng of Li deposited at the cone orifice after cleaning with 2% HNO_3 for 5 min, which is of the same magnitude as the total Li deposition (231.2 ng) after exposure to the Li solution alone (Fig. 3). These findings demonstrate that 2% HNO_3 is not an efficient cleaning solution for removing Li deposits at the cone orifice. This suggests that Li-containing deposits progressively accumulate on the cone surfaces and are influenced by the Li isotope composition of the preceding sample during Li isotope analysis. This accumulation leads to an increase in background Li signals over time, thereby contributing to the observed memory effect.

3.3 Optimal type and concentration of eluent

To mitigate the memory effect of Li during Li isotopic analysis, a 5% NaCl cleaning method has been identified as the most effective solution. This method decreases the Li background signal by two orders of magnitude without significantly diminishing the Li signal intensity, with efficacy persisting for up to 3 h.[36] This method has been widely adopted in practice, and has undergone iterative refinements by various researchers. The 5% NaCl cleaning method can effectively reduce Li memory effect, and the maintenance time of such a low Li background can be extended from 3 to 6 h.[81,82] Without NaCl cleaning, the Li background rapidly rises to 100 mV, whereas the Li background can be reduced to 0.5 mV by employing the NaCl cleaning method.[39] In addition, 10 ng per g of NaCl solution effectively mitigate the Li memory effect.[39] A 0.3% NaCl solution significantly reduces the Li memory effect during isotope analysis using Nu Plasma MC-ICP-MS.[53]

Although NaCl can eliminate the Li memory effect, some researchers suggest reducing the concentration of NaCl used. This is because an excessively high NaCl concentration will block the nebulizer and induce matrix effects induced by Na. However, an insufficient NaCl concentration fails to form an effective coating based on the surface-coating mechanism proposed by Lin *et al.*,[36] rendering the method inadequate to eliminate the memory effect. Thus, determining an optimal NaCl concentration is essential for enhancing the applicability of this technique.

To identify the optimal concentration of NaCl for mitigating the Li memory effect, varying concentrations of NaCl solutions

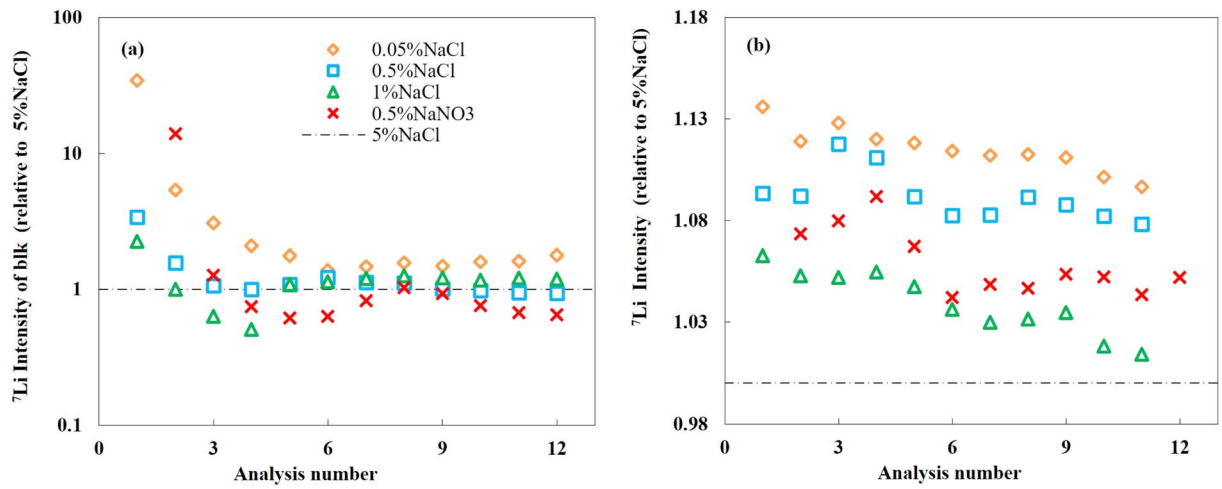

Fig. 3 Verification of optimal NaCl concentration and the effectiveness of $NaNO_3$. (a) ^7Li intensity of background and (b) ^7Li intensity.

were evaluated as eluents: 0.05%, 0.5%, 1%, and 5%. The cleaning procedure involved the following steps: initially, a 100 ng per g L-SVEC solution was introduced into the MC-ICP-MS, with instrument parameters optimized to generate a ^{7}Li signal of ~12 V. After 5 h of continuous injection to induce the memory effect, the system was cleaned with NaCl eluents for 5 min, followed by a 5-minute rinse with 2% HNO_3. Subsequently, the Li background signal was recorded. Following cleaning with NaCl eluents of varying concentrations (0.05%, 0.5%, 1%, and 5%) and 2% HNO_3, the respective Li background signals were 17.0 ± 1.7 (2SD, n = 6) mV, 10.5 ± 3.7 (2SD, n = 6) mV, 13.0 ± 4.2 (2SD, n = 6) mV, and 10.8 ± 2.2 (2SD, n = 6) mV (Fig. 3a). Corresponding signal-to-noise ratios (SNRs) were 720.8 ± 68.1 (2SD, n = 6), 1200.9 ± 455.2 (2SD, n = 6), 862.9 ± 190.1 (2SD, n = 6), and 1105.4 ± 225.5 (2SD, n = 6). In contrast, cleaning only with 2% HNO_3 yielded a Li background of 119.9 ± 13.4 (2SD, n = 5) mV and a SNR of 49.9 ± 5.1 (2SD, n = 5) (Table 3).

These results indicate that each concentration of NaCl solution effectively reduced the Li memory effect. Although higher NaCl concentrations provided superior memory effect mitigation, they pose an increased risk of nebulizer clogging and signal attenuation due to sample extraction inefficiency (Fig. 3b). Normalized data relative to the 5% NaCl + 2% HNO_3 combination reveal that 0.05% and 1% NaCl demonstrate inferior cleaning effects compared to 5% NaCl, although they induce less signal suppression. The 0.5% NaCl solution achieved the most effective memory effect reduction with relatively minimal signal attenuation (Fig. 3). Thus, the optimal cleaning performance was attained with 0.5% NaCl considering the

Table 3 Background (mV) and signal-to-noise ratio (SNR) of ^{7}Li under different cleaning solutions

Elute	^{7}Li blk (mV)	Intensity (V)	SNR
2% HNO_3	119.9 ± 0.0 (2SD, n = 5) mV	5.7 ± 0.0 (2SD, n = 169)	49.9 ± 5.1 (2SD, n = 5)
0.05% NaCl → 2% HNO_3	17.0 ± 1.7 (2SD, n = 6) mV	12.4 ± 0.4 (2SD, n = 174)	720.8 ± 68.1 (2SD, n = 6)
0.5% NaCl → 2% HNO_3	10.5 ± 3.7 (2SD, n = 6) mV	12.1 ± 0.4 (2SD, n = 179)	1200.9 ± 455.2 (2SD, n = 6)
1% NaCl → 2% HNO_3	13.0 ± 4.2 (2SD, n = 6) mV	11.5 ± 0.2 (2SD, n = 213)	862.9 ± 190.1 (2SD, n = 6)
5% NaCl → 2% HNO_3	10.8 ± 2.2 (2SD, n = 6) mV	11.1 ± 0.5 (2SD, n = 176)	1105.4 ± 225.5 (2SD, n = 6)
0.5% $NaNO_3$ → 2% HNO_3	9.6 ± 4.9 (2SD, n = 6) mV	11.8 ± 0.4 (2SD, n = 195)	1317.8 ± 684.1 (2SD, n = 6)

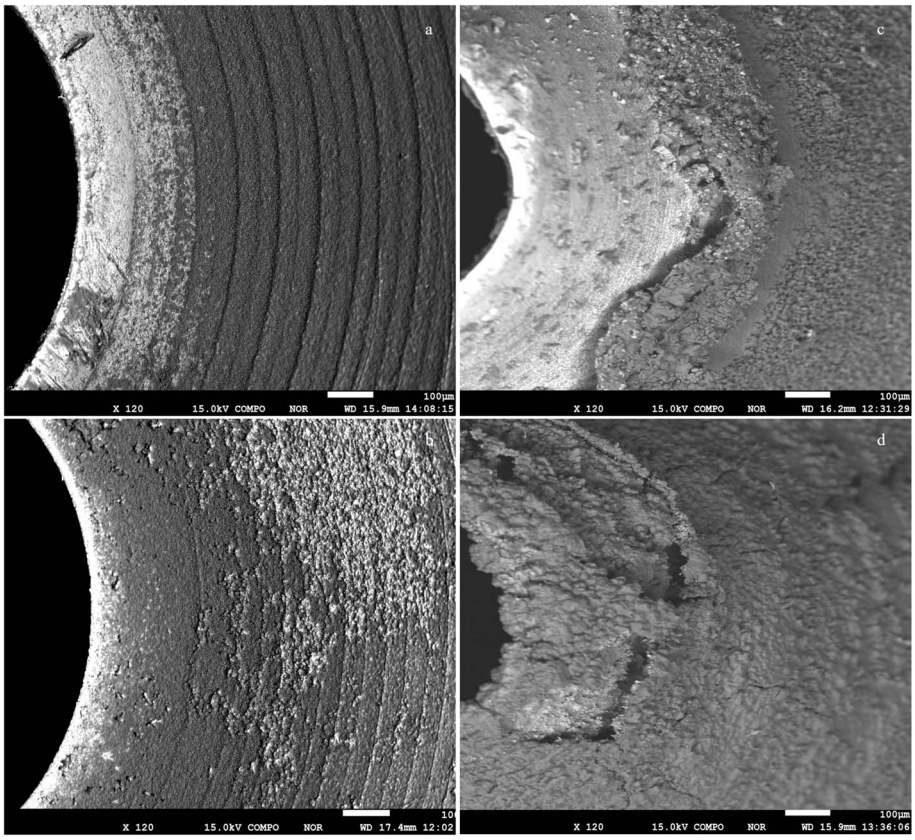

Fig. 4 Exterior surfaces of the sampling cone (left) and skimmer cone (right) after the introduction of different solutions as follows: (a and c) 5 minutes of 5% NaCl and (b and d) 1 hour of 200 ng per g L-SVEC followed by 5 minutes of 5% NaCl.

balance between memory effect reduction and signal suppression.

In addition to considering the reasonable concentration of NaCl, we also tested the appropriate type of the eluent. This is because Cl^- may introduce spectral interferences, such as the $^{40}Ar^{35}Cl$, $^{35}Cl^{16}O$, $^{37}Cl^{16}O$, and $^{40}Ar^{37}Cl$, potentially affect the detection of ^{75}As, ^{51}V, ^{53}Cr and ^{77}Se, respectively.[83–85] In contrast, the nitrogen (N) and oxygen (O) components in $NaNO_3$ are primarily derived from atmospheric sources and do not introduce additional interferences. From an interference reduction perspective, $NaNO_3$ is a more suitable cleaning agent.

The efficacy of $NaNO_3$ was evaluated using solutions with the same concentrations as NaCl. Using a 0.5% $NaNO_3$ solution, the ^7Li background signal was reduced to 9.6 ± 4.9 mV (2SD, $n = 6$), with a SNR of 1317.8 ± 684.1 (2SD, $n = 6$), surpassing the memory effect mitigation performance of the 0.5% NaCl solution (Table 3 and Fig. 3). Considering both interference reduction and signal attenuation, 0.5% $NaNO_3$ is deemed more suitable than NaCl.

3.4 Elucidating the mechanism of the Na solution in reducing the memory effect

To investigate the mechanism by which NaCl solutions reduce the Li memory effect, three new sets of sample and skimmer cones were selected, and experiments were conducted using two different solutions. For the first set of cones, a 5% NaCl solution was introduced for 5 minutes to assess whether NaCl could form a "Na film" on the cone surfaces (Fig. 4a). The second set of cones was exposed to a 200 ng per g L-SVEC solution for 1 hour, followed by a 5% NaCl rinse for 5 minutes to examine whether NaCl reduces the memory effect by flushing Li deposits from the cones (Fig. 4b).

The SEM observations revealed that a "Na film" formed at the orifices of the sampling and skimmer cones after introducing the 5% NaCl solution for 5 min, with more extensive deposition observed on the skimmer cone (Fig. 4a and c). When a Li solution was introduced prior to the NaCl solution, uniform deposition layers were observed at the cone orifices, suggesting that the NaCl film was superimposed on existing Li deposits (Fig. 4b and d). Elution experiments indicated that introducing NaCl after a Li solution did not significantly reduce the Li content on the cones, with Li levels remaining at 225.7 ng compared to 231.2 ng (Li-only condition). These findings indicate that the NaCl solution does not flush away Li deposits; instead, it forms a coating that completely encapsulates them. Detailed SEM analysis revealed that the "Na film" formed by the NaCl solution consists of a nano-coating composed of spherical particles at the nanometer scale (Fig. 5a). This structure resembles the micro/nano-architecture of lotus leaf surfaces (Fig. 5c and d) known for their hydrophobic and self-cleaning properties,[86] similar to the SiO_2 layer formed by the introduction of Si solutions, which reduces the memory effect by creating a dense particle layer.[55] Thus, we inferred that the NaCl

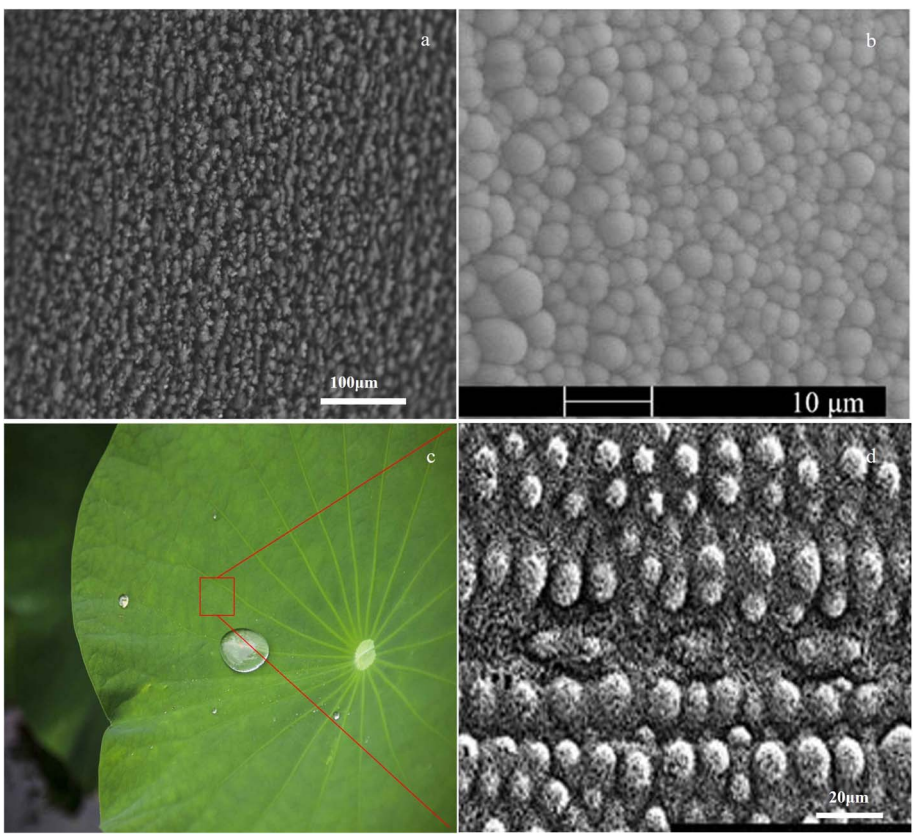

Fig. 5 (a) NaCl nano-particle coating and the hydrophobicity of lotus leaf surfaces; (b) SiO_2 nano-particle coating; and (c and d) SEM observations of the micro–nano structure of lotus leaf surfaces (modified from Barthlott *et al.*).[86]

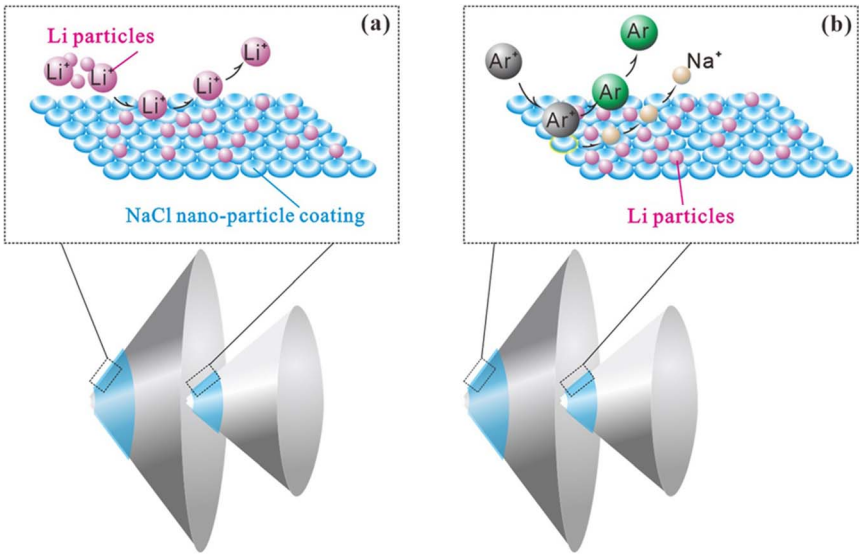

Fig. 6 Elucidating the reduction in the memory effect of Li by the addition of Na solution. (a) Sodium chloride nanoparticle coating. (b) Preferential ionization of sodium ions.

film consisted of nano-particles that can minimize the deposition of analyzed Li to reduce the Li memory effect.

The Li memory effect arises from the deposition and subsequent re-ionization of Li on the cones. To further eliminate the Li memory effect, it is necessary to inhibit deposition and re-ionization. Bohlin *et al.*[39] proposed that alkali and alkaline earth metal solutions could theoretically reduce the Li memory effect. Lee *et al.*[63] reported that introducing a 1000 ng per g Be solution for 2 min effectively reduces the memory effect during trace element determination by ICP-MS. However, the mechanism remains unclear. We hypothesize that the low ionization energies of alkali and alkaline earth metals enable them to form coatings on the cones, and these coatings preferentially ionize under the influence of discrete Ar^+ ions. As a result, the Li ionization is suppressed. The lower first ionization energy of Na compared with Li (5.14 *vs.* 5.39 eV) means that Na preferentially ionizes, thereby reducing the re-ionization of deposited Li.

To verify this hypothesis, experiments were conducted using potassium (K) as a cleaning eluent since it has an even lower ionization energy (4.34 eV). Different concentrations of KCl solutions (0.05%, 0.5%, 1%, and 5%) were tested for their ability to mitigate the Li memory effect. Additionally, 5% NaCl and 5% KCl were tested on the element XR, and varying concentrations of KCl were compared with 5% NaCl on the MC-ICP-MS (ESI Fig. S1 and S2†). KCl solutions were more effective than NaCl in reducing the Li memory effect, with Li SNRs improving by 1.2–5.4 times. However, KCl solutions caused signal suppression of 6–29%, which gradually recovered after prolonged Li solution introduction.

In summary, the NaCl solution reduces the Li memory effect through the formation of a nano-structured coating that limits redeposition and re-ionization of Li analytes. Deposition Reduction: A micro/nano-coating formed by high-concentrations of NaCl reduces the deposition of Li on cone surfaces (Fig. 6a). Re-ionization suppression: Na preferentially ionizes over Li owing to its lower ionization energy to prevent Li re-ionization (Fig. 6b).

4. Conclusion

We provide a comprehensive analysis of the Li memory effect on the determination of Li isotopic composition. It was confirmed that the primary location of the Li memory effect lies within the skimmer and sampling cones through SEM observations and cone elution experiments. Conditional experiments further demonstrated that 0.5% $NaNO_3$ is an optimal cleaning solution, as it effectively reduces the Li memory effect while avoiding Cl^- related mass spectrometry interferences, offering a practical alternative to NaCl solutions. The mechanism by which Na-based solutions mitigate the memory effect was explored *via* SEM, cone elution and KCl rinsing experiments. The findings suggest that the nano-coating formed by Na-based solutions at the cone orifice reduces the redeposition and re-ionization of Li analytes. These findings are applicable to Li isotopic analysis by SN-MC-ICP-MS and hold significant value for Li isotopic determination by LA-MC-ICP-MS and Li content analysis by ICP-MS. Moreover, this research can provide valuable insights into mitigating memory effects of other elements.

Data availability

The authors declare that the data supporting the findings of this study are available within the paper and its ESI files.† Should any raw data files be needed in another format, they are available from the corresponding author upon reasonable request. Source data are provided with this paper.

Conflicts of interest

There are no conflicts to declare.

Acknowledgements

This work was funded by the National Natural Science Foundation of China (42473038), MOST (Ministry of Science and Technology) Special Fund from the State Key Laboratory of Geological Processes and Mineral Resources (MSFGPMR01), the Natural Science Foundation of Hubei Province (2020CFA045) and the Fundamental Research Funds for the Central Universities, China University of Geosciences (Wuhan).

References

1 R. Findlay, E. T. Tipper, C. R. Walton, O. Shorttle, M. A. Sephton, R. Martins, K. M. M. Shaw, J. Hu, A. Knight, M. Tarique, W. J. McMahon and H. M. Williams, *Meteorit. Planet. Sci.*, 2024, **59**, A127.
2 Y. Gong, C. Y. Liu, Y. Liu, L. Lei, M. Xiang, B. Yang, Z. Zhou, Y. Zhang, X. R. Yang, L. Yan and Y. Xiong, *Minerals*, 2024, **14**, 735.
3 J. P. Helper, J. D. Barnes, J. M. de Moor, A. Rodriguez, S. Agostini, G. Segee-Wright, R. Chatterjee and D. F. Stockli, *Geochim. Cosmochim. Acta*, 2024, **377**, 52–67.
4 Y. J. Lin, M. Merli, P. Censi, S. A. T. Redfern, Y. Zhao, Q. Z. Yin, M. P. Zheng, X. D. Yu, Y. S. Zhang, W. J. Knapp and E. T. Tipper, *Geochim. Cosmochim. Acta*, 2024, **374**, 250–263.
5 M. Luo, M. G. Yu, M. E. Torres, E. A. Solomon, J. Gieskes, C. F. You, L. R. Kong and D. F. Chen, *Earth Planet. Sci. Lett.*, 2024, **642**, 118854.
6 Z. L. Ma, Y. Tang, Y. P. Su, Z. H. Lv, X. Zhang and H. Zhang, *Lithos*, 2024, **482**, 107731.
7 G. H. Qin, J. H. Wei, Y. C. Wei, D. Y. Cao, X. Li and Y. Zhang, *Minerals*, 2024, **14**, 836.
8 W. H. Wu, Y. T. Guan, W. Nel and C. X. Xu, *Appl. Geochem.*, 2024, **175**, 106163.
9 H. B. Zhao, W. L. Miao, X. Y. Zhang and W. X. Li, *Aquat. Geochem.*, 2024, **30**, 179–199.
10 J. A. Zhong, Y. J. Lin, F. M. Wang, K. L. Su, Z. Liu, D. B. Sheng, H. B. Li and B. Pang, *Aquat. Geochem.*, 2024, **30**, 163–178.
11 C. Brant, L. A. Coogan, K. M. Gillis, W. E. Seyfried, N. J. Pester and J. Spence, *Geochim. Cosmochim. Acta*, 2012, **96**, 272–293.
12 T. Elliott, A. Thomas, A. Jeffcoate and Y. L. Niu, *Nature*, 2006, **443**, 565–568.
13 S. Misra and P. N. Froelich, *Science*, 2012, **335**, 818–823.
14 R. L. Rudnick and D. A. Ionov, *Earth Planet. Sci. Lett.*, 2007, **256**, 278–293.
15 P. A. E. Pogge von Strandmann, H. C. Jenkyns and R. G. Woodfine, *Nat. Geosci.*, 2013, **6**, 668–672.
16 J. Lin, A. Yang, R. Lin, J. Mao, Z. Hu and Y. Liu, *J. Earth Sci.*, 2023, **34**, 1663–1691.
17 L. Xing, X. Yilin, N. Olivier, L. Dongyong, L. Haiyang, Z. Zhang and H. Zhenhui, *J. Earth Sci.*, 2022, **33**, 1–37.
18 Y. Xiangying, L. Bin, T. Dongbo, L. Kecheng, Z. Zhiyong, S. Hafiz Muhammad and X. Yilin, *J. Earth Sci.*, 2024, **35**, 1878–1894.
19 C. Cao, T. Li, T. Y. Chen, G. J. Li, W. Li and J. Chen, *J. Anal. At. Spectrom.*, 2023, **38**, 1602–1610.
20 Y. Hu and F. Z. Teng, *J. Anal. At. Spectrom.*, 2019, **34**, 338–346.
21 A. Winckelmann, D. Morcillo, S. Richter, S. Recknagel, J. Riedel, J. Vogl, U. Panne and C. Abad, *Anal. Bioanal. Chem.*, 2022, **414**, 251–256.
22 Y. Y. Cheng, G. N. Li, Y. Z. Li, L. Deng, M. Y. He, L. B. Y. Liu, J. X. Luo and Z. D. Jin, *Bull. Mineral., Petrol. Geochem.*, 2023, **42**, 369–379.
23 L. F. Gou, Z. D. Jin, L. Deng, H. Sun, H. M. Yu and F. Zhang, *Geochemistry*, 2017, **46**, 528–537.
24 M. Y. He, C. g. Luo, H. Lu, Z. d. Jin and L. Deng, *J. Anal. At. Spectrom.*, 2019, **34**, 1773–1778.
25 A. B. Jeffcoate, T. Elliott, A. Thomas and C. Bouman, *Geostand. Geoanal. Res.*, 2004, **28**, 161–172.
26 C. J. Bryant, M. T. McCulloch and V. C. Bennett, *J. Anal. At. Spectrom.*, 2003, **18**, 734–737.
27 P. B. Tomascak, *Rev. Mineral. Geochem.*, 2004, **55**, 153–195.
28 Z. Y. Zhu, T. Yang and X. K. Zhu, *J. Anal. At. Spectrom.*, 2019, **34**, 1503–1513.
29 P. B. Tomascak, F. Tera, R. T. Helz and R. J. Walker, *Geochim. Cosmochim. Acta*, 1999, **63**, 907–910.
30 R. Millot, C. Guerrot and N. Vigier, *Geostand. Geoanal. Res.*, 2004, **28**, 153–159.
31 S. Misra and P. N. Froelich, *J. Anal. At. Spectrom.*, 2009, **24**, 1524–1533.
32 K. J. Hou, Y. H. Li, Y. K. Xiao, F. Liu and Y. R. Tian, *Chin. Sci. Bull.*, 2010, **55**, 3305–3311.
33 J. Lin, Y. S. Liu, L. Y. Zhu, W. Zhang and Z. C. Hu, *Spectrochim. Acta, Part B*, 2021, **177**, 106074.
34 X. M. Liu and W. S. Li, *J. Anal. At. Spectrom.*, 2019, **34**, 1708–1717.
35 L. F. Gou, Z. D. Jin, L. Deng, M. Y. He and C. Y. Liu, *Spectrochim. Acta, Part B*, 2018, **146**, 1–8.
36 J. Lin, Y. S. Liu, Z. C. Hu, L. Yang, K. Chen, H. H. Chen, K. Q. Zong and S. Gao, *J. Anal. At. Spectrom.*, 2016, **31**, 390–397.
37 M. Adloff, A. Ridgwell, F. M. Monteiro, I. J. Parkinson, A. J. Dickson, P. von Strandmann, M. S. Fantle and S. E. Greene, *Geosci. Model Dev.*, 2021, **14**, 4187–4223.
38 S. L. Badea, V. C. Niculescu and A. M. Iordache, *Materials*, 2023, **16**, 3817.
39 M. S. Bohlin, S. Misra, N. Lloyd, H. Elderfield and M. J. Bickle, *Rapid Commun. Mass Spectrom.*, 2018, **32**, 93–104.
40 H. Chang, Y. J. Zhao, P. Hu, G. Y. Zhou, W. X. Zhang, L. Zhou, J. Lin, Z. C. Hu and Y. B. Wu, *Chem. Geol.*, 2024, **661**, 122188.
41 H. R. Duan, Z. Y. Zhu, C. X. Pan, J. X. Ma, Z. Y. Long and K. F. Qiu, *At. Spectrosc.*, 2023, **44**, 198–206.
42 J. K. Golla, J. Bouchez and J. L. Druhan, *Geophys. Res. Lett.*, 2024, **51**, 1–11.
43 J. W. Lee, H. S. Min, J. Kim and K. S. Lee, *Accredit. Qual. Assur.*, 2024, **30**, 117–128.
44 D. Morcillo, A. Winckelmann, D. A. Frick, L. Jacobsen, T. Seger, S. Florek, S. Richter, J. Vogl, S. Recknagel, U. Panne and C. Adab, *Spectrochim. Acta, Part B*, 2024, **220**, 107013.
45 M. S. Navarro, G. M. Paula-Santos, T. D. Marteleto and J. Enzweiler, *Geostand. Geoanal. Res.*, 2021, **45**, 701–718.

46 I. Pessoa, B. Cunha, L. Antonioli, M. Coelho, A. Tavares, L. Romero and A. Moterani, *Appl. Spectrosc.*, 2022, **76**, 1440–1451.
47 L. F. Gou, C. Y. Liu, L. Deng and Z. D. Jin, *Rapid Commun. Mass Spectrom.*, 2020, **34**, e8577.
48 X. Q. Li, G. L. Han, Q. Zhang, R. Qu and Z. Miao, *Spectrochim. Acta, Part B*, 2022, **188**, 106348.
49 T. T. Phan, A. N. P. Vankeuren and J. A. Hakala, *Int. J. Coal Geol.*, 2018, **191**, 95–111.
50 F. Thibon, L. Weppe, M. Montanes, P. Telouk and N. Vigier, *J. Anal. At. Spectrom.*, 2021, **36**, 1381.
51 L. Xu, C. G. Luo and H. J. Wen, *Geostand. Geoanal. Res.*, 2020, **44**, 201–214.
52 T. T. Phan, J. A. Hakala and S. Sharma, *Sci. Total Environ.*, 2020, **714**, 136867.
53 Q. Tang, L. Chen, S. Tian, W. Hu, Y. Gong and Y. Zi, *Rock Miner. Anal.*, 2024, **43**, 201–212.
54 J. Carter, L. Ebdon and E. H. Evans, *J. Anal. At. Spectrom.*, 2003, **18**, 142–145.
55 H. Kipphardt, M. Czerwensky and R. Matschat, *J. Anal. At. Spectrom.*, 2005, **20**, 28–34.
56 J. S. de Gois, M. Costas-Rodríguez, P. Vallelonga, D. L. G. Borges and F. Vanhaecke, *J. Anal. At. Spectrom.*, 2016, **31**, 537–542.
57 H. Chen, N. J. Saunders, M. Jerram and A. N. Halliday, *Chem. Geol.*, 2021, **578**, 120281.
58 S. Tian, E. C. Inglis, J. B. Creech, W. Zhang, Z. Wang, Z. Hu, Y. Liu and F. Moynier, *Chem. Geol.*, 2020, **555**, 119791.
59 I. Rodushkin, E. Engström and D. C. Baxter, *Anal. Bioanal. Chem.*, 2010, **396**, 365–377.
60 S. F. Boulyga, A. Koepf, S. Konegger-Kappel, Z. Macsik and G. Stadelmann, *J. Anal. At. Spectrom.*, 2016, **31**, 2272–2284.
61 I. Rodushkin and F. Ödman, *J. Trace Elem. Med. Biol.*, 2001, **14**, 241–247.
62 E. Engström, A. Stenberg, S. Senioukh, R. Edelbro, D. C. Baxter and I. Rodushkin, *Anal. Chim. Acta*, 2004, **521**, 123–135.
63 J. W. Lee, H. S. Min, J. Kim and K.-S. Lee, *Accredit. Qual. Assur.*, 2024, **30**, 117–128.
64 Y. Liu, Z. Hu, S. Gao, D. Günther, J. Xu, C. Gao and H. Chen, *Chem. Geol.*, 2008, **257**, 34–43.
65 J. Lin, Y. S. Liu, Z. C. Hu, W. Chen, L. Zhang and H. H. Chen, *Geostand. Geoanal. Res.*, 2019, **43**, 277–289.
66 P. B. Tomascak, R. W. Carlson and S. B. Shirey, *Chem. Geol.*, 1999, **158**, 145–154.
67 M. A. Elburg, P. Vroon and A. Scherstén, *J. Anal. At. Spectrom.*, 2005, **20**, 1389.
68 M. T. McCulloch, M. Holcomb, K. Rankenburg and J. A. Trotter, *Rapid Commun. Mass Spectrom.*, 2014, **28**, 2704–2712.
69 Y. J. Tang, H. F. Zhang, E. Nakamura, T. Moriguti, K. Kobayashi and J. F. Ying, *Geochim. Cosmochim. Acta*, 2007, **71**, 4327–4341.
70 J.-I. Kimura, Q. Chang, T. Ishikawa and T. Tsujimori, *J. Anal. At. Spectrom.*, 2016, **31**, 2305–2320.
71 D. J. Douglas and L. A. Kerr, *J. Anal. At. Spectrom.*, 1988, **3**, 749–752.
72 Y. Nishio and S. Nakai, *Anal. Chim. Acta*, 2002, **456**, 271–281.
73 G. J. Wei, J. X. Wei, Y. Liu, T. Ke, Z. Y. Ren, J. L. Ma and Y. G. Xu, *J. Anal. At. Spectrom.*, 2013, **28**, 606–612.
74 C. W. Magee Jr and C. A. Norris, *Geosci. Instrum., Methods Data Syst.*, 2015, **4**, 75–80.
75 D. W. Boomer and M. J. Powell, *Anal. Chem.*, 1987, **59**, 2810–2813.
76 H. Andrén, I. Rodushkin, A. Stenberg, D. Malinovsky and D. C. Baxter, *J. Anal. At. Spectrom.*, 2004, **19**, 1217–1224.
77 Y. H. Yang and H. F. Zhang, *J. Mass Spectrom. Soc.*, 2005, **41**, 64–73.
78 H. B. Lim, R. S. Houk, M. C. Edelson and K. P. Carney, *J. Anal. At. Spectrom.*, 1989, **4**, 365–370.
79 N. Taylor and P. B. Farnsworth, *Spectrochim. Acta, Part B*, 2012, **69**, 2–8.
80 C. Agatemor and D. Beauchemin, *Anal. Chim. Acta*, 2011, **706**, 66–83.
81 T. T. Phan, J. A. Hakala and S. Sharma, *Sci. Total Environ.*, 2020, **714**, 136867.
82 T. T. Phan, A. N. Paukert Vankeuren and J. A. Hakala, *Int. J. Coal Geol.*, 2018, **191**, 95–111.
83 L. Jiang and Z. Yin, *J. Environ. Hyg.*, 2013, **3**, 369–372.
84 J. Karasiński, C. T. Nguyen-Marcińczyk, M. Wojciechowski, E. Bulska and L. Halicz, *J. Anal. At. Spectrom.*, 2020, **35**, 560–566.
85 S. Schuth, I. Horn, A. Brüske, P. E. Wolff and S. Weyer, *Ore Geol. Rev.*, 2017, **81**, 1271–1286.
86 W. Barthlott and C. Neinhuis, *Planta*, 1997, **202**, 1–8.